Applied Physics Express 7, 031002 (2014)
http://dx.doi.org/10.7567/APEX.7.031002

Impact of CF_4 plasma treatment on threshold voltage and mobility in Al_2O_3/InAlN/GaN MOSHEMTs

Zongyang Hu[1*], Yuanzheng Yue[1], Mingda Zhu[1], Bo Song[1], Satyaki Ganguly[1], Josh Bergman[2], Debdeep Jena[1], and Huili Grace Xing[1*]

[1]Department of Electrical Engineering, University of Notre Dame, Notre Dame, IN 46556, U.S.A.
[2]Teledyne Scientific and Imaging, LLC, Thousand Oaks, CA 91360, U.S.A.
E-mail: zhu1@nd.edu; hxing@nd.edu

Received January 7, 2014; accepted February 3, 2014; published online February 20, 2014

The shift of the threshold voltage V_{th} in Al_2O_3/InAlN/GaN metal–oxide–semiconductor high-electron-mobility transistors (MOSHEMTs) is demonstrated by CF_4 plasma treatments. The accompanying channel mobility degradation is monitored to understand the tradeoff design space. The effective negative charge introduced by the F plasma treatments at the oxide interface is found to be as high as $-0.73 \times 10^{13}\,cm^{-2}$ (mobility > 500 $cm^2\,V^{-1}\,s^{-1}$), sufficient to fully compensate for the net polarization charge in $Al_{0.15}GaN$/GaN HEMTs. Although it is difficult to obtain $V_{th} \gg 0$ V owing to the high polarization charges in InAlN, these MOSHEMTs with 1 µm gates show very low leakage (~1×10^{-11} A/mm), low hysteresis, and low dispersion. © 2014 The Japan Society of Applied Physics

GaN high-electron-mobility transistors (HEMTs) with a lattice-matched $In_{0.17}Al_{0.83}N$ barrier have been extensively studied for high-power and high-speed applications in recent years. Compared with the low-Al-composition AlGaN barrier, the $In_{0.17}Al_{0.83}N$ barrier offers higher two-dimensional electron gas (2DEG) densities with lower barrier thicknesses, and InAlN HEMTs have shown superior performance in terms of output current, on-resistance, and current gain cutoff frequency.[1–3] In principle, enhancement mode (E-mode) operation is more challenging for InAlN barrier HEMTs than AlGaN barrier HEMTs because of the following aspects: (1) a high threshold voltage V_{th} as well as precise control of the threshold voltage is harder to achieve owing to the large polarization charge, and thus, the 2DEG concentration; (2) the channel carrier mobility is more prone to degradation owing to the thin barriers (<10 nm) when scattering centers are introduced during device fabrication;[4,5] (3) gate leakage could be high owing to the intrinsically large spontaneous polarization field and barrier height fluctuation.[6] As a means to reduce the gate leakage, various gate dielectrics have been studied for metal–oxide–semiconductor (MOS) HEMTs, among which Al_2O_3 seems to provide a reasonable combination of decent band gap, dielectric constant, breakdown electric field, and low interfacial states with InAlN.[7] Despite these advantages, it is often observed that Al_2O_3 induces positive sheet charges at the interface with (InAlGa)N barriers,[8] which suggests that E-mode operation is difficult to achieve by a pure gate recess technique in MOSHEMTs. On the other hand, negative charges can be introduced by fluorine-containing plasma treatments;[9–11] furthermore, if the F-induced negative charge largely compensates for the interfacial positive charge, the E-mode operation is expected, and V_{th} can increase with increasing gate dielectric thickness.[8] Recently, successful demonstrations of E-mode MOSHEMTs using an AlGaN barrier with high threshold voltages ($V_{th} > 2$ V) have been reported.[12–14] However, for InAlN barrier MOSHEMTs, there have been very few reports on the E-mode operation owing to the challenges mentioned above. Moreover, a detailed study on V_{th} control and electron transport properties is still lacking for a comprehensive evaluation of this technique.

In this work, we investigated CF_4 plasma treatments of thin-InAlN-barrier (5 nm) GaN MOSHEMTs on their effectiveness in compensating for the positive interface charge. The MOSHEMTs demonstrated here show E-mode operation with extremely low leakage currents and very small hysteresis and dispersion. On the basis of the measured current–voltage (I–V) and capacitance–voltage (C–V) characteristics, the interface properties and electron mobility in the channel are extracted. A tradeoff between V_{th} and carrier peak mobility is observed.

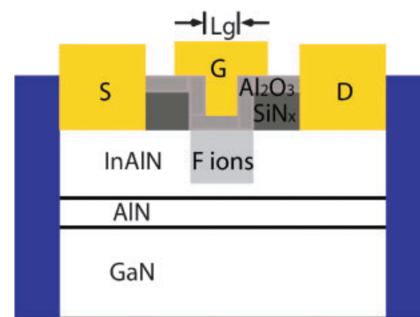

Fig. 1. Cross-sectional schematic of Al_2O_3/InAlN/GaN MOSHEMTs.

The HEMT structure (Fig. 1) consists of a 5 nm $In_{0.17}Al_{0.83}N$ top barrier, a 1 nm AlN interlayer, a GaN channel, and a 1.8 µm semi-insulating GaN buffer on a SiC substrate grown by metal organic chemical vapor deposition at IQE RF LLC. Alloyed ohmic contacts and device isolation using ion implantation were formed first, followed by a blanket SiN_x (25 nm) deposition. CF_4 plasma at 40 W in a reactive ion etch (RIE) system was used to etch SiN_x for 2.5 min at an etch rate of 30 nm/min for defining the gate foot region. F plasma treatments were subsequently carried out using a similar CF_4 plasma condition for 3 min but at high power settings: 60, 80, and 100 W. The etch rate of InAlN in CF_4 plasma was measured by atomic force microscopy (AFM); an etch rate of <0.2 nm/min was extracted for the 40 W CF_4 plasma, and a maximum etch rate of 0.5 nm/min was observed at the highest plasma power of 100 W. As a result, the remaining InAlN barrier thickness is expected to be >3 nm in all the MOSHEMTs in this study; devices that received the CF_4 plasma etching of SiN_x at 40 W only are referred to as MOSHEMTs with unintentional (UI) F plasma treatment. Following the F plasma treatment, the HEMT samples received low-power O_2 plasma cleaning and rinsing in

© 2014 The Japan Society of Applied Physics

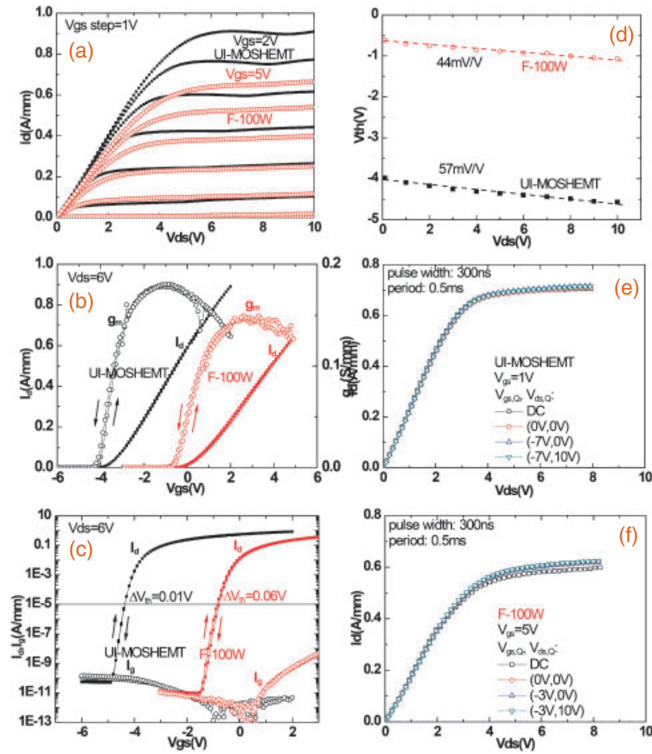

Fig. 2. Example of device DC characteristics of MOSHEMTs with unintentional and 100 W F plasma treatments: (a) I_d–V_{ds}; dual sweep of transfer characteristics at $V_{ds} = 6$ V (b) in linear scale and (c) in semilog scale; (d) V_{th} (determined at $I_d = 10\,\mu$A/mm) as a function of V_{ds}; (e) and (f) pulsed I–V measurements with 300 ns pulse width and 0.5 ms period. For both devices, $L_g = 1\,\mu$m, $L_{sd} = 4\,\mu$m, and the Al_2O_3 thickness is 16 nm.

diluted HCl prior to the gate dielectric deposition of Al_2O_3 with different thicknesses by atomic layer deposition (ALD). Amorphous Al_2O_3 is well known to etch in tetramethylammonium hydroxide (TMAH), which is commonly used in photoresist developers. To prevent the accidental etching of the ALD Al_2O_3 gate dielectric in the subsequent processing steps, 20 nm SiN_x was deposited by plasma-enhanced chemical vapor deposition (PECVD) as a protective layer. After gate lithography and prior to gate metallization, this layer of SiN_x was removed using CF_4 plasma at 40 W. The gate metal extends 0.5 µm on both the source and drain sides over the gate foot for a complete coverage of the treated gate area. The devices were annealed at 400 °C for 5 min after gate metallization to reverse the ion damage caused by the CF_4 plasma treatment[15] as well as improve the oxide interfaces. A cross-sectional schematic of finished devices is shown in Fig. 1 along with the process flow.

Examples of DC I–V characteristics are plotted in Fig. 2 for MOSHEMTs with UI and intentional F plasma treatments. Both devices have a gate length (L_g) of 1 µm, a source–drain distance (L_{sd}) of 4 µm, and a gate oxide (Al_2O_3) thickness of 16 nm. The device with intentional F plasma treatment received CF_4 plasma at 100 W for 3 min, thus termed as F-100W in Fig. 2. A drain current of 0.9 A/mm is measured for the UI-MOSHEMT at $V_{gs} = 2$ V and 0.6 A/mm for the F-100W MOSHEMT at $V_{gs} = 5$ V. Dual-sweep transfer I–Vs at $V_{ds} = 6$ V [Figs. 2(b) and 2(c)] show minimal hysteresis in both devices in both the on-state and subthreshold region, which indicates negligible oxide interface state density underneath the gate. The peak transconductances g_m are 180 and 150 mS/mm for the UI and F-100W MOSHEMTs, respectively. In Fig. 2(c), it is also shown that the off-state leakage currents are as low as 1×10^{-11} A/mm; therefore, a very high current on/off ratio of $\sim 10^{11}$ is observed. This low leakage current can be ascribed to (1) high-quality gate dielectrics and (2) excellent interdevice isolation using ion implantation.

The device threshold voltage is defined at $I_d = 10\,\mu$A/mm. The hysteresis at V_{th} is as low as 0.01 V for the device with unintentional F plasma treatment and 0.06 V for the device with 100 W F plasma treatment [Fig. 2(c)]. The same criterion applies to all V_{th} and hysteresis extracted in this work. By changing V_{ds} from 0.1 to 10 V, the values of the drain-induced barrier lowering (DIBL) effect are measured to be 57 and 44 mV/V for the two types of device, which are satisfactorily low for a total barrier thickness of ~20 nm and L_g of 1 µm. It is observed that the MOSHEMT V_{th} is shifted by 3.5 V with the 100 W CF_4 plasma treatment and 16 nm Al_2O_3. Pulsed I–V characteristics with a 300 ns pulse width and a 0.5 ms period are shown in Figs. 2(e) and 2(f). Negligible current collapse is observed under pulsed gate and pulsed drain bias conditions for both UI-MOSHEMT and F-100W-MOSHEMT, further confirming the low trap density underneath the gate and the effective passivation in the access region.

The device V_{th} values of MOSHEMTs with different plasma powers and gate oxide thicknesses are summarized in Fig. 3(a). Errors in V_{th} were estimated by comparing a group of MOSHEMTs with nominally the same geometry and treatments, which is found to be <0.1 V. An example is shown in Figs. 4(b) and 4(c): the dual-sweep transfer I–Vs of 4 MOSHEMTs showing V_{th} at 10 µA/mm are reasonably uniform, and the measurement error is well within 0.1 V considering both hysteresis and variation across different devices. It is found that V_{th} of devices that received the same plasma power decreases (becoming more negative) with increasing oxide thickness in a nearly linear fashion. Furthermore, the magnitude of the fitted slope decreases with increasing plasma power, which in turn suggests that the electric field in the gate oxide at V_{th} is reduced by the fluorine plasma treatment.

To gain physical insight, we have modeled V_{th} of the MOSHEMT shown in Fig. 1(a) as

$$V_{th} = \phi_b - \frac{(Q_{it} + Q_F - \sigma_{GaN})t_{ox}}{\varepsilon_{Al_2O_3}} - \frac{\Delta E_{c,Al_2O_3/InAlN}}{e} - \frac{\sigma_{InAlN/GaN}t_{InAlN}}{\varepsilon_{InAlN}} - \frac{\sigma_{AlN/GaN}t_{AlN}}{\varepsilon_{AlN}} - \frac{\Delta E_{c,InAlN/GaN}}{e} + \frac{\Delta E_0}{e} + \Delta V_F. \quad (1)$$

In Eq. (1), the constants include ϕ_b—the barrier height between gate metal and Al_2O_3, $\Delta E_{c,Al_2O_3/InAlN}$ ($\Delta E_{c,InAlN/GaN}$)—the conduction band offset between Al_2O_3 and InAlN (InAlN and GaN), ΔE_0—the energy difference between the Fermi level and the conduction band of the GaN channel, $\sigma_{InAlN/GaN}$ ($\sigma_{AlN/GaN}$)—the polarization charge difference between InAlN and GaN (AlN and GaN), and σ_{GaN}—the spontaneous polarization charge in GaN. The parameters include the following: Q_{it}—the interface sheet charge density at the Al_2O_3/InAlN interface, Q_F—the

 © 2014 The Japan Society of Applied Physics

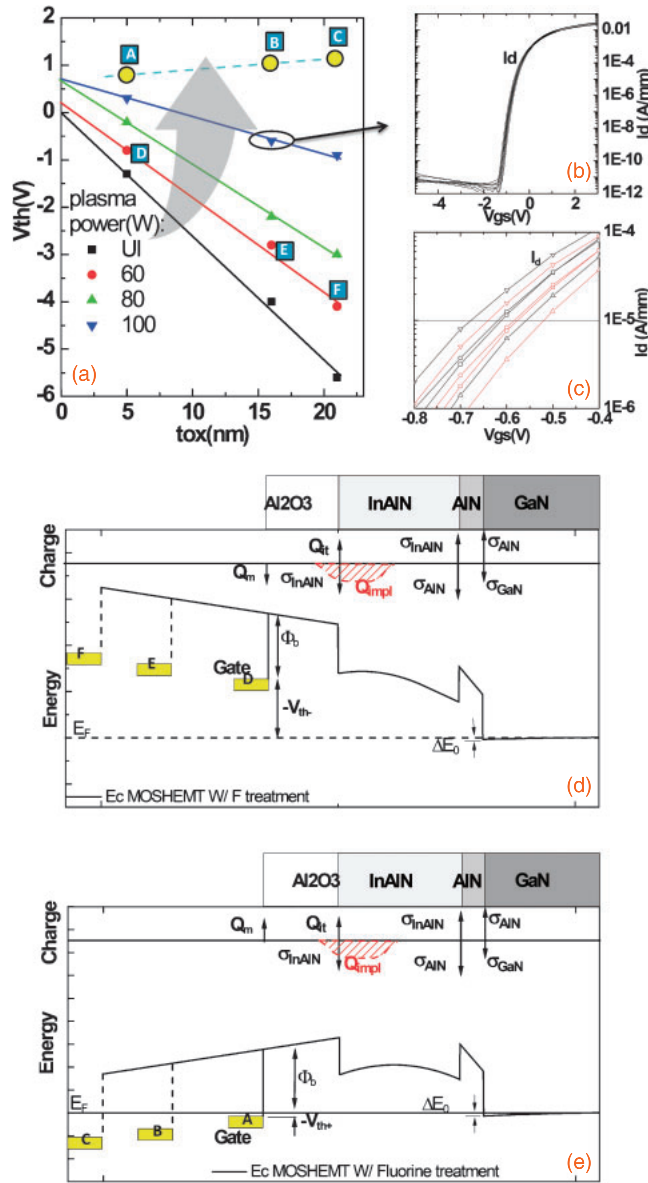

Fig. 3. (a) Threshold voltages of MOSHEMTs ($L_g \sim 20\,\mu$m) as functions of gate oxide thickness and CF_4 plasma power. Solid lines are for V_{th} calculated according to the model. Examples of uniform V_{th} in MOSHEMTs in this work: (b) transfer I–V and (c) zoomed-in transfer I–V plots of four different devices with the same geometries and plasma treatment. Energy band diagrams when (d) $Q_{it} + Q_F > \sigma_{GaN}$, thus, a negative electric field in the oxide and a decreasing V_{th} with increasing t_{ox}, and (e) $Q_{it} + Q_F < \sigma_{GaN}$, thus, a positive electric field in the oxide and an increasing V_{th} with increasing t_{ox}. In (d) and (e), the sheet charge Q_F in Eq. (1) is represented by the spatially distributed charges Q_{impl} implanted during the F plasma treatment.

equivalent interface charge introduced by CF_4 plasma treatment located at the Al_2O_3/InAlN interface, t — the thickness of each layer of the MOSHEMT top barrier, and ΔV_F that captures the other effects due to F ion spatial distribution and possible modification of band offset.

On the basis of the magnitude of the negative charges introduced in the top barrier, the electric field in the gate oxide at V_{th} can be either negative or positive. The energy band diagrams of these two cases are shown in Figs. 3(d) and 3(e), where the equivalent sheet charge Q_F in Eq. (1) is replaced by the spatially distributed Q_{impl} to reflect the realistic F ion profile due to the plasma treatments. The case of a positive electric field in the gate oxide [corresponding to a positive slope of V_{th} vs t_{ox} in Fig. 3(a)] is depicted in Fig. 3(e), which is the desired situation since V_{th} is positive and increases with increasing gate oxide thickness [Situations A–C in Figs. 3(a) and 3(e)]. Experimentally, we only observed the situation depicted in Fig. 3(d), where V_{th} decreases with increasing t_{ox} [Situations D–E in Figs. 3(a) and 3(d)]. On the basis of this understanding and the linear fitting of the measured V_{th}, it can be concluded that $Q_{it} + Q_F$ is modified by treatments with different F plasma powers, but it shows negligible dependence on the gate oxide thickness. Q_{it} can originate from two sources: fixed interface charge Q_{fix} and occupation of interface states qD_{it}. Since all the devices show negligible hysteresis and the Fermi level at the oxide/InAlN interface at V_{th} for devices with the same InAlN barrier is independent of the gate oxide thickness [see Figs. 3(d) and 3(e)], Q_{it} should be the same for this group of MOSHEMTs. As a result, we can infer that a high F plasma power leads to a high equivalent fluorine negative charge Q_F.

According to Eq. (1), the shift of V_{th} can be divided into three parts: (1) band bending in the gate oxide owing to the presence of Q_F, thus modified electric field in the oxide [the second term in Eq. (1) is extractable from the slopes in Fig. 3(a)]; (2) thinning of the InAlN barrier owing to its finite etch in CF_4 plasma [the fourth term in Eq. (1) is computable from the etch rate calibration]; (3) change in conduction band offset and band bending arising from F ion distribution in the oxide and InAlN. [the last term in Eq. (1)]. On the basis of this understanding, the contribution breakdown of ΔV_{th} is summarized in Fig. 4(a). The total equivalent interface charge $Q_{it} + Q_F$, extracted from the linear slopes in Fig. 3(a), reduces from $2.84 \times 10^{13}\,\text{cm}^{-2}$ in UI-MOSHEMTs to $2.11 \times 10^{13}\,\text{cm}^{-2}$ in F-100W MOSHEMTs, approaching the spontaneous polarization charge density of GaN $\sigma_{GaN} = 1.81 \times 10^{13}\,\text{cm}^{-2}$,[16] when a zero electric field in the gate oxide at V_{th}

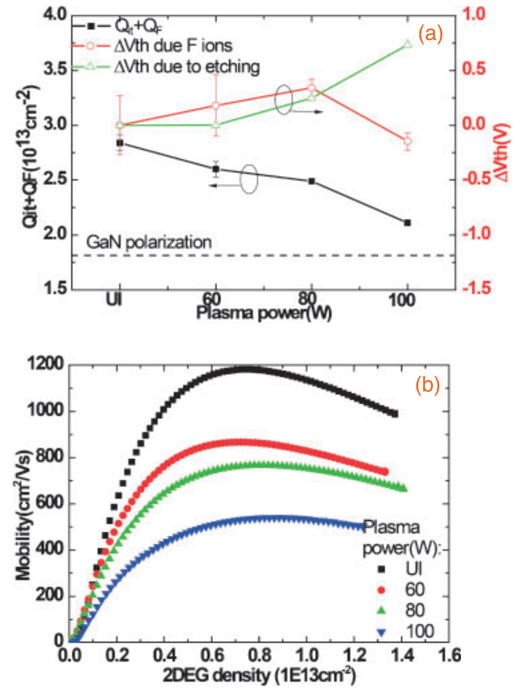

Fig. 4. (a) $Q_{it} + Q_F$ and V_{th} shift due to barrier thinning and other effects extracted using Eq. (1); (b) electron mobility in the channel extracted by the split C–V method as a function of F plasma power and 2DEG density.

© 2014 The Japan Society of Applied Physics

is expected. The interface charge $Q_{it} + Q_F$ in the UI-MOSHEMTs is found to be positive and very close to $\sigma_{InAlN/GaN} \sim 2.7 \times 10^{13}\,cm^{-2}$ despite the unintentional F plasma treatment at 40 W and the post-gate annealing. F plasma treatments at a power higher than 40 W clearly introduced net negative charges in the barrier with an effective sheet concentration of $\sim 0.73 \times 10^{13}\,cm^{-2}$ at 100 W. This amount of negative charge could have led to a positive slope in V_{th} as a function of t_{ox} [Situations A–C in Fig. 3(e)] if AlGaN with 15% Al composition is used as the barrier material, using the same assumption $Q_{it} \sim \sigma_{AlGaN/GaN}$. Reversal of the electric field direction in the gate oxide is not observed in this experiment, which is most probably due to the large Q_{it} ($\sim \sigma_{InAlN/GaN}$) at the Al_2O_3/InAlN barrier. Subtracting the shift of V_{th} due to InAlN thinning from the intercepts of the fitted lines on the V_{th} axis, we can obtain ΔV_{th} due to the aforementioned other effects. A drop in ΔV_{th} due to other effects is observed at 100 W, which needs further investigation. Other than this anomalous point, it is observed that the F plasma treatment helps in shifting V_{th} partially due to the incorporation of negative charges and partially due to the thinning of the barrier. This observation is so far consistent with previous reports.[12,17)]

To evaluate the adverse effect of the F plasma treatment, electron mobility in the channel is extracted by the split *C–V* method.[18)] The MOSHEMT transfer characteristics were measured at $V_{ds} = 0.1\,V$, and the *C–V* characteristics of the same MOSHEMT were measured at 1 MHz. To minimize errors in L_g owing to the gate extension over SiN_x (see Fig. 1), MOSHEMTs with a 20-µm-long gate are used. The extracted mobility as a function of 2DEG density and F plasma power is plotted in Fig. 4(b). The electron mobility for the UI-MOSHEMT has a peak value of $1180\,cm^2\,V^{-1}\,s^{-1}$ near a 2DEG density of $7 \times 10^{12}\,cm^{-2}$ and decreases with increasing 2DEG density largely owing to enhanced interface roughness scattering.[19)] The fast decrease in mobility at low 2DEG densities is most likely a result of charged dislocation scattering and remote ionized impurity scattering mechanisms.[5,20)] The peak mobility decreases with increasing F plasma power, which is expected owing to the escalated charged impurity scattering. The peak mobility is $\sim 540\,cm^2\,V^{-1}\,s^{-1}$ near $8 \times 10^{12}\,cm^{-2}$ for the F-100W MOSHEMT. The reduced channel mobility, together with the higher hysteresis in the F-100W MOSHEMT (see Fig. 2) than in the UI-MOSHEMT, suggests that a further increase in F plasma power might not be desirable for improving device performance.

In summary, Al_2O_3/InAlN/GaN MOSHEMTs with a 5 nm InAlN barrier fabricated in this work show encouraging performance in terms of low leakage current (1×10^{-11} A/mm), low hysteresis (60 mV), and E-mode operation ($V_{th} \sim 0.5\,V$ defined at $I_d = 10\,\mu A/mm$). CF_4 plasma treatment is observed to introduce net negative charges in the MOSHEMT gate barrier, thus leading to a positive shift in V_{th} together with the barrier thinning. However, a further increase in V_{th} without severe degradation of the channel mobility is shown to be difficult owing to the large polarization charge of InAlN. Improvements in I_d and g_m can be expected in F-plasma-treated AlGaN/GaN HEMTs (for lower polarization charge under the gate) and capped with InAlN in the access region (for lower access resistance).

Acknowledgments This work was supported by the DARPA-MPC program, monitored by John Albrecht, Daniel Green, and Paul Maki.

1) Y. Yue, Z. Hu, J. Guo, B. Sensale-Rodriguez, G. Li, R. Wang, F. Faria, T. Fang, B. Song, X. Gao, S. Guo, T. Kosel, G. Snider, P. Fay, D. Jena, and H. Xing, IEEE Electron Device Lett. **33**, 988 (2012).
2) H. Sun, A. R. Alt, H. Benedickter, E. Feltin, J.-F. Carlin, M. Gonschorek, N. Grandjean, and C. R. Bolognesi, IEEE Electron Device Lett. **31**, 293 (2010).
3) M. L. Schuette, A. Ketterson, B. Song, E. Beam, T.-M. Chou, M. Pilla, H.-Q. Tserng, X. Gao, S. Guo, P. J. Fay, H. G. Xing, and P. Saunier, IEEE Electron Device Lett. **34**, 741 (2013).
4) Y. Cao, H. Xing, and D. Jena, Appl. Phys. Lett. **97**, 222116 (2010).
5) T.-H. Hung, M. Esposto, and S. Rajan, Appl. Phys. Lett. **99**, 162104 (2011).
6) S. Ganguly, A. Konar, Z. Hu, H. Xing, and D. Jena, Appl. Phys. Lett. **101**, 253519 (2012).
7) K. Čičo, K. Hušeková, M. Ťapajna, D. Gregušová, R. Stoklas, J. Kuzmík, J.-F. Carlin, N. Grandjean, D. Pogany, and K. Fröhlich, J. Vac. Sci. Technol. B **29**, 01A808 (2011).
8) S. Ganguly, J. Verma, G. Li, T. Zimmermann, H. Xing, and D. Jena, Appl. Phys. Lett. **99**, 193504 (2011).
9) Y. Cai, Y. Zhou, K. J. Chen, and K. M. Lau, IEEE Electron Device Lett. **26**, 435 (2005).
10) R. Wang, Y. Cai, C.-W. Tang, K. M. Lau, and K. J. Chen, IEEE Electron Device Lett. **27**, 793 (2006).
11) F. Medjdoub, M. Alomari, J.-F. Carlin, M. Gonschorek, E. Feltin, M. A. Py, C. Gaquiere, N. Grandjean, and E. Kohn, Electron. Lett. **44**, 696 (2008).
12) Y. Zhang, M. Sun, S. J. Joglekar, T. Fujishima, and T. Palacios, Appl. Phys. Lett. **103**, 033524 (2013).
13) Y. Wang, M. Wang, B. Xie, C. P. Wen, J. Wang, Y. Hao, W. Wu, K. J. Chen, and B. Shen, IEEE Electron Device Lett. **34**, 1370 (2013).
14) Z. Tang, Q. Jiang, Y. Lu, S. Huang, S. Yang, X. Tang, and K. J. Chen, IEEE Electron Device Lett. **34**, 1373 (2013).
15) Y. Cai, Y. Zhou, K. M. Lau, and K. J. Chen, IEEE Trans. Electron Devices **53**, 2207 (2006).
16) O. Ambacher, J. Smart, J. R. Shealy, N. G. Weimann, K. Chu, M. Murphy, W. J. Schaff, L. F. Eastman, R. Dimitrov, L. Wittmer, M. Stutzmann, W. Rieger, and J. Hilsenbeck, J. Appl. Phys. **85**, 3222 (1999).
17) R. Chu, C. S. Suh, M. H. Wong, N. Fichtenbaum, D. Brown, L. McCarthy, S. Keller, F. Wu, J. S. Speck, and U. K. Mishra, IEEE Electron Device Lett. **28**, 781 (2007).
18) K. Romanjek, F. Andrieu, T. Ernst, and G. Ghibaudo, IEEE Electron Device Lett. **25**, 583 (2004).
19) Y. Cao and D. Jena, Appl. Phys. Lett. **90**, 182112 (2007).
20) D. Jena, A. C. Gossard, and U. K. Mishra, Appl. Phys. Lett. **76**, 1707 (2000).

© 2014 The Japan Society of Applied Physics